Intrinsic Pinning of Vorticity by Domain Walls of $\hat{\mathbf{l}}$ Texture in Superfluid ^{3}He-*A*

P. M. Walmsley, I. J. White, and A. I. Golov

Department of Physics and Astronomy, Manchester University, Manchester, United Kingdom

(Received 10 August 2004; published 5 November 2004)

We present the first observation of substantial persistent flow in superfluid ^{3}He-*A* in thick simply connected slabs in a zero magnetic field, but only in $\hat{\mathbf{l}}$ textures with domain walls. The flow is induced in a rotating cryostat using a torsional oscillator as a probe. The hysteretic dependences of the trapped vorticity on the maximal angular velocity of rotation are fairly universal for different densities of domain walls and slab thicknesses. A model of a critical state set by either the critical velocity for vortex nucleation or pinning strength explains all observations.

DOI: 10.1103/PhysRevLett.93.195301 PACS numbers: 67.57.De, 47.32.–y, 67.57.Fg, 74.25.Qt

Pinning of vortices in type-II superconductors or superfluid ^{4}He by *extrinsic* inhomogeneities such as crystal defects or roughness of container walls is an important issue in both fundamental studies of vortex matter [1,2] and applied research on high nondissipative currents [3] and strong permanent magnets [4]. However, in chiral superconductors and superfluids *intrinsic* pinning is also possible in which a vorticity-carrying state of an anisotropic multicomponent order parameter is metastable. For example, in Sr_2RuO_4 singular vortices can be trapped by domain walls between differently oriented ground states [5,6] even with little extrinsic disorder. In this Letter, we present observations of strong trapping of continuous vortices in superfluid ^{3}He-*A* by stable defects of its order parameter (and only weak trapping without defects) and models of the relevant critical states. We have also, for the first time, observed persistent currents in ^{3}He-*A* in wide channels and in zero magnetic field.

^{3}He-*A* is a chiral fermionic *p*-wave superfluid whose order parameter can be specified locally by two orthogonal unit vectors $\hat{\mathbf{m}}$ and $\hat{\mathbf{n}}$ (such that $\hat{\mathbf{l}} \equiv \hat{\mathbf{m}} \times \hat{\mathbf{n}}$ points in the direction of the orbital momentum of Cooper pairs) and a unit vector $\hat{\mathbf{d}}$ (spin quantization axis) [7]. Unlike other superfluids, where the global phase enforces quantization of circulation and hence topological stability of the superflow, in ^{3}He-*A* spatial variation of the orbital vectors (texture) determines the superfluid velocity as

$$\mathbf{v}_s = \frac{\kappa_0}{2\pi} \sum_j \hat{m}_j \nabla \hat{n}_j,$$

where $\kappa_0 \equiv h/2m_3$ is the quantum of circulation. Hence, ^{3}He-*A* allows vortices with *continuous* cores (where nonzero $\nabla \times \mathbf{v}_s$ does not imply suppression but only reorientation of the order parameter) which have the lowest critical velocity for nucleation [8,9]. Three-dimensional reorientation of the $\hat{\mathbf{l}}$ texture in time will cause gradual decay of superflow without the need for discrete phase slips due to moving singular vortices. This orbital motion (and hence dissipation) can be suppressed by placing ^{3}He-*A* in either channels thinner than the dipole healing length $\xi_d \simeq 10\ \mu$m or in a magnetic field above $H_d \simeq 20$ G. While superflow in ^{3}He-*A* in narrow channels was shown to persist [10,11], no evidence of a persistent flow in wide channels and zero field has been demonstrated so far.

We studied ^{3}He-*A* in thick slabs in zero field. The rotational symmetry is broken by the boundary conditions that align $\hat{\mathbf{l}}$ vectors with the normal to the walls, $\hat{\mathbf{z}}$, and by the dipole-locking alignment of $\hat{\mathbf{d}}$ with $\pm\hat{\mathbf{l}}$ leaving a discrete spectrum of $\hat{\mathbf{l}}$ and $\hat{\mathbf{d}}$ vectors ($\hat{l}_z = \pm 1$, $\hat{d}_z = \pm 1$). Hence, the ground state is a fourfold degenerate uniform texture normal to the slab walls [12]. The corresponding topological defects are domain walls separating ground states with different orientations of $\hat{\mathbf{l}}$ and $\hat{\mathbf{d}}$. There are three types: "ld wall" (dipole-locked, both $\hat{\mathbf{l}}$ and $\hat{\mathbf{d}}$ vectors flip), "l wall" (only $\hat{\mathbf{l}}$ vector flips) and "d wall" (only $\hat{\mathbf{d}}$ vector flips); see Fig. 1.

If we rotate the slab at angular velocity $\mathbf{\Omega} \parallel \hat{\mathbf{z}}$, continuous vortices (which are another type of topological defect of the $\hat{\mathbf{l}}$ texture) will nucleate after the counterflow near the rim exceeds the critical value v_c. In a uniform $\hat{\mathbf{l}}$ texture, these will be two-quantum vortices [13] with

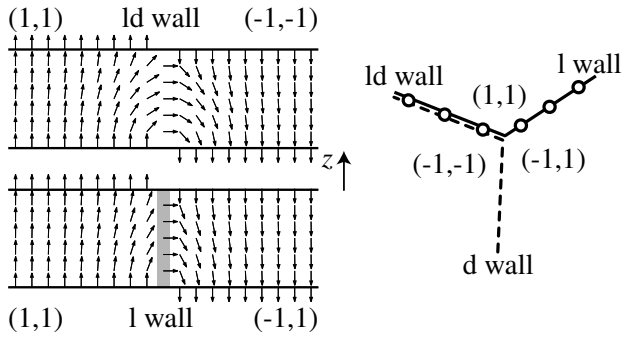

FIG. 1. Left panel: Side views of the $\hat{\mathbf{l}}$ texture in two types of domain walls in a slab; the different ground states far from the walls are labeled by $(\hat{l}_z, \hat{d}_z)$: ld wall ($\hat{\mathbf{l}} = \hat{\mathbf{d}}$ everywhere) and l wall ($\hat{\mathbf{l}} = \hat{\mathbf{d}}$ on the left, $\hat{\mathbf{l}} = -\hat{\mathbf{d}}$ on the right, and $\hat{\mathbf{l}} \neq \hat{\mathbf{d}}$ in the shaded region of width $\sim\xi_d$. Right panel: Schematic top view of a stable three-way junction of all three types of domain walls; it might possess the trap for the vortices (shown by circles) on ld and l walls.

$v_c \sim 0.5$ mm/s [9]. However, in the presence of a domain wall separating two ground states with opposite orientation of $\hat{\mathbf{l}}$ (Fig. 2), kinks in the wall, which are single-quantum vortices themselves, can be nucleated at a smaller critical velocity ($v_c \sim 0.15$–0.25 mm/s [9,14]). A domain wall decorated with vorticity is called a vortex sheet [8,13,15]; it was observed that vortices are transported along the sheet. Both ld walls and l walls can carry vorticity; however, vortex energies should generally differ between them, producing a barrier for vortex propagation from one type of wall to another (Fig. 1). In both cases the vorticity is localized on the wall within the region of disturbed $\hat{\mathbf{l}}$ texture of order of the slab thickness D outside which the texture is uniform and $\nabla \times \mathbf{v}_s = 0$.

For ^{3}He-A in a container with smooth walls, thanks to the large length scale of $\hat{\mathbf{l}}$-texture deformation, the extrinsic disorder can be neglected and neither thermal nor quantum fluctuations are important. Hence, only intrinsic processes such as hydrodynamic instabilities are relevant to continuous vorticity. Thus, in the same experimental cell we can have either uniform $\hat{\mathbf{l}}$ textures (they are obtained only after cooling through T_c at continuous rotation that provides directional bias for $\hat{\mathbf{l}}$) or different densities of l walls and ld walls (obtained either by cooling through T_c without rotation or warming up from the B phase). This differs from the situation in superconductors and other superfluids where quenched inhomogeneities (e.g., grain boundaries) exist independently of superconductivity. In ^{3}He-A both vortices and domain walls are defects of the same superfluid order parameter. One can think of vortex nucleation and trapping as flow-induced first-order transitions between different stable nonuniform textures of the multicomponent order parameter.

We studied textures in two disk-shaped slabs of radius $R = 5.0$ mm and thicknesses $D = 0.26$ and 0.44 mm. To eliminate extrinsic pinning, the walls were made of polished Stycast 1266. The 8 mm-long 0.9 mm i.d. Be-Cu fill capillary entered the disk on its axis and also served as the torsion rod and thermal link to the ^{3}He in the nuclear stage. The resonant frequency ν_R and bandwidth ν_B of the torsional oscillator (TO) were tracked electrostatically as in [9]. The ^{3}He-A was held at a pressure of 29.3 bar and the temperature 2.0–2.5 mK was determined *in situ* by measuring $\rho_s(T)$ with the TO.

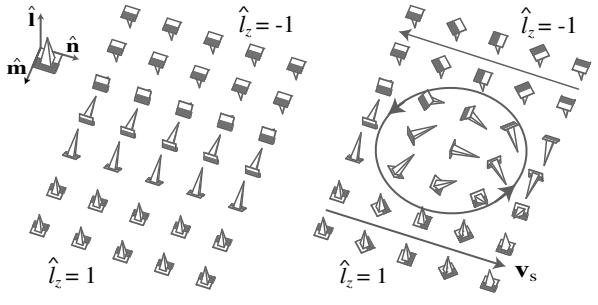

FIG. 2. The variation of the orbital triad $(\hat{\mathbf{m}}, \hat{\mathbf{n}}, \hat{\mathbf{l}})$ in the middle of the slab for either ld wall or l wall without vorticity (left) and with one quantum of circulation (right).

The technique of monitoring the presence of vortices is the same as in [9]. The ν_R and ν_B of the TO are mainly sensitive to the orientation of the $\hat{\mathbf{l}}$ texture near the rim of the disk through the anisotropy of the density and viscosity of the normal component. The texture in turn responds (by tipping azimuthally) to the azimuthal counterflow $v(R)$ after the latter exceeds the Fréedericksz velocity $v_F \simeq \sqrt{5}\kappa_0/4D$ [9]. Thus, the ν_R is the highest (and ν_B is the smallest) when the counterflow is zero near the rim, $v(R) = 0$. The azimuthal dc flow of the normal component $v_n(R) = \Omega R$ was induced by the continuous rotation of the cryostat. The superfluid velocity $v_s(R) = N\kappa_0/2\pi R$ is a function of the total number of circulation quanta N. Then $v(R) \equiv v_n(R) - v_s(R) = \Omega R - N\kappa_0/2\pi R$. In the presence of N_{trap} trapped quanta of circulation, $v(R) = 0$ when the cryostat rotates at $\Omega_{\text{trap}} = N_{\text{trap}}\kappa_0/2\pi R^2$. We hence measure N_{trap} by determining the corresponding Ω_{trap} at which ν_R is a maximum and ν_B is a minimum (see Fig. 3).

The samples of different initial textures were prepared as follows. Uniform oriented normal $\hat{\mathbf{l}}$ textures were obtained by cooling through T_c while rotating at $\Omega \simeq 0.4$ rad/s (this direction of rotation was then deemed positive). The textures with a moderate number of domain walls were produced by slow cooling through T_c without rotation ("$N \rightarrow A$"), and those with a large number of domain walls were obtained after warming from the B phase ("$B \rightarrow A$"). The higher density of domain walls in

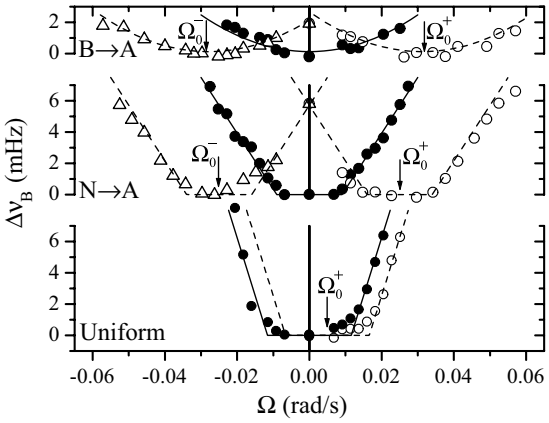

FIG. 3. The shift in ν_B versus Ω in three different textures for $D = 0.44$ mm showing the offset by Ω_0 in the flow-induced Fréedericksz transition caused by the trapped circulation. Key: ●, no trapped vorticity; ○, after rotating at $\Omega = 0.5$ rad/s in positive direction; △, after rotating at $\Omega = -0.5$ rad/s in negative direction. Solid lines through the data are mirror symmetric about $\Omega = 0$. The results of their translation by Ω_0 are given by the dashed lines.

$B \rightarrow A$ textures can be independently confirmed by the smearing of the flow-induced Fréedericksz transition (Fig. 3).

Sweeps of rotation from $\Omega = 0$ to $\Omega_{\max}$ and back revealed that after $\Omega_{\max}$ exceeded $\Omega_c \equiv v_c/R \sim 0.1$ rad/s (i.e., vortices were introduced) the dependencies of ν_R and ν_B on small Ω got shifted by a certain Ω_{trap}. For sweeps up to $\Omega_{\max} \gg \Omega_c$ it saturated at a value Ω_0 (Fig. 3). The value of Ω_0 reversed after the cryostat rotated in the opposite direction. Even in uniform textures nonzero $N_{\text{trap}} \sim 10$ was observed. However, in $N \rightarrow A$ and $B \rightarrow A$ textures maximal N_{trap} was always between 50 and 70. No decay of Ω_0 was observed after 3 days. We also observed no temperature dependence.

The dependence of Ω_{trap} on the history of rotation in $N \rightarrow A$ and $B \rightarrow A$ is shown in Fig. 4, which is our major result. Each data point is taken after rotating the cryostat at Ω_{prep} (and hence introducing $N = 2\pi R(\Omega_{\text{prep}}R - v_c)/\kappa_0$ quanta of circulation, e.g., $N = 600$ at $\Omega_{\text{prep}} = 0.5$ rad/s) and then stopping and checking the value of Ω_{trap} as in Fig. 3. This is analogous to measuring magnetization loops in superconductors or ferromagnets (i.e., remanent magnetization after exposing the material to a certain magnetic field). To improve the reproducibility of the hysteresis loops, we initially "trained" these samples by rotating at $\Omega = 0.5$ rad/s in both directions; this apparently helped speed up coarsening and relaxation of the web of domain walls. The striking fact is that all loops taken in slabs of both thicknesses and for different densities of domain walls are essentially identical. Above $|\Omega_{\text{prep}}| = 0.1$ rad/s they all saturate at the value $|\Omega_0| = 0.026 \pm 0.004$ rad/s comparable to the critical angular velocity for vortex nucleation $\Omega_c \approx 0.03$ rad/s.

However, the very different responses of uniform textures to rotation are shown in Fig. 5. They are characterized by higher Ω_c but much smaller Ω_0. The loops are asymmetric for rotation in positive and negative direction because uniform textures are *oriented*. While such a texture is stable against rotation in the positive direction, it is usually destroyed irreversibly after being rotated in the opposite direction beyond the corresponding $\Omega_c^- \approx -0.04$ rad/s [13]. This is apparently due to the creation and expansion of new domains of differently oriented $\hat{\mathbf{l}}$ texture after the vortices of the opposite orientation were nucleated. Therefore we always first measured $\Omega_{\text{trap}}(\Omega_{\text{prep}})$ for $\Omega_{\text{prep}} > 0$. One can notice that while Ω_c decreases with increasing slab thickness, the values of Ω_0 are the same for both slabs. The trapped $N_{\text{trap}} \approx 10$ quanta of circulation could be removed by slow rotation in the opposite direction to some $\Omega_p \approx -\Omega_0$ (this is why the left branch of $\Delta\nu_B(\Omega)$ in Fig. 3 could not be measured at constant $N_{\text{trap}} > 0$). Then no new vortices would appear if the cryostat rotated at any Ω such that $\Omega_c^- < \Omega < \Omega_c$. This can be used to prepare samples completely free of remanent vorticity. We believe that the trapped vortices were the double-quantum vortices weakly pinned by either residual surface roughness or some pinned d walls.

Two different processes can change the vorticity in the sample: *nucleation* of new vortices when local counterflow v exceeds v_c and *unpinning* of existing vortices by the Magnus force $F_M = \rho_s \kappa_0 v$. If we quantify the critical pinning force F_p by the equivalent Magnus force F_M, then the convenient parameter is the "unpinning velocity" $v_p \equiv F_p/\rho_s\kappa_0$. In this framework, to calculate the maximal possible number of remanent vortices after stopping rotation we should find out what will happen first in the critical state at the rim: unpinning of an existing vortex at $|v| > v_p$ or nucleation of an antivortex at $|v| > v_c$. Hence, there are two possibilities:

(i) Strong pinning ($v_p > v_c$): limitation by antivortex creation $|v_s(R)| \leq v_c$. In this case, the upper limit of Ω_{trap}

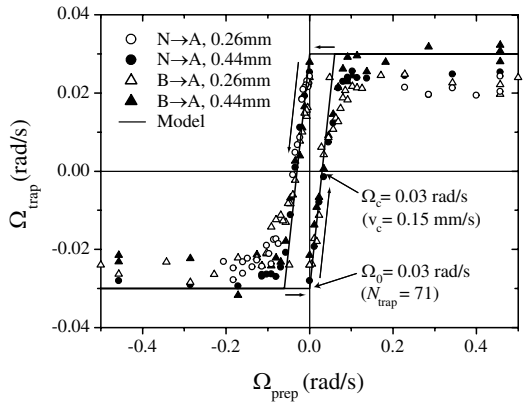

FIG. 4. Hysteretic dependencies of Ω_{trap} on Ω_{prep} for $N \rightarrow A$ and $B \rightarrow A$ textures in both slabs along with the model prediction for strong pinning with $\Omega_c = 0.03$ rad/s (solid line).

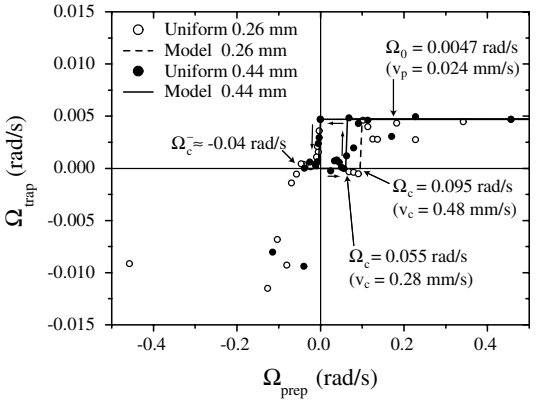

FIG. 5. Hysteretic Ω_{trap} versus Ω_{prep} for textures that were initially uniform at $\Omega_{\text{prep}} > \Omega_c^- \approx -0.04$ rad/s but further rotation at $\Omega_{\text{prep}} < \Omega_c^-$ introduced domain walls. Two model predictions for weak pinning are given for the same $v_p = 0.024$ mm/s but different critical velocities: $v_c = 0.48$ mm/s (dashed line) and $v_c = 0.28$ mm/s (solid line).

is $\Omega_0 = \Omega_c = v_c/R$. The resulting model line for $v_c = 0.15$ mm/s, shown in Fig. 4, is in good agreement with the data. Both horizontal (Ω_c) and vertical (Ω_0) scales are set by v_c (which is nearly the same for domain walls in both slabs). The particular value of v_p is irrelevant as well as the actual distribution of the pinning centers and the details of the mechanism of unpinning (collective versus individual). This naturally explains the observed universality of the hysteretic loops in samples purposely prepared with enough domain walls.

(ii) Weak pinning ($v_p < v_c$): limitation by the pinning force $|v_s(R)| \leq v_p$ (but only if there are vortices, otherwise $|v_s(R)| \leq v_c$ again). In this case, the upper limit of Ω_{trap} is $\Omega_0 = v_p/R$. Then the fact that both slabs revealed identical values of $\Omega_0 = 0.0047$ rad/s (corresponding to $v_p = 0.024$ mm/s) might indicate a common origin of the pinning mechanisms in both slabs. The resulting model lines for two sets of parameters suitable to describe the data for both slabs are shown in Fig. 5. Now both parameters v_p and v_c matter, and the loops have a peculiar shape with the plateau of $\Omega_{\text{trap}} = 0$ for $-v_c^-/R < \Omega_{\text{prep}} < -v_p/R$, in agreement with the experimental observation.

In chiral p-wave superconductors anomalously strong pining of vortices was observed in zero-field-cooled samples (and only weak pinning in field-cooled ones) [6]. In these, the spectrum of possible orientations of $\hat{\mathbf{l}}$ is also discrete due to the locking of $\hat{\mathbf{l}}$ to the crystal-field anisotropy. Zero-field-cooled samples should possess multiple domain walls of the order parameter and are hence direct analogs of ^{3}He-A in a slab cooled through T_c without rotation ($N \rightarrow A$). Sigrist and Agterberg speculated that some vortices can be trapped on domain walls (which are pinned by lattice defects themselves) and repel the others [5]. We would like to suggest another scenario when vortices exist only as mobile kinks on l walls and ld walls, but experience potential barriers at wall junctions.

The domain walls always appear if ^{3}He-A is cooled from the normal phase at $\Omega = 0$, and they are hard to remove [13]. Apparently, the emerging order parameter of ^{3}He-A in different regions of the slab spontaneously acquires independent orientation of $\hat{\mathbf{l}}$ and $\hat{\mathbf{d}}$ vectors, and hence upon coarsening ends up with a mosaic of domains of all four possible ground states. These will be separated by a web of all three types of domain walls; the only common type of junction is a three-way vertex depicted in Fig. 1. Such a "polycrystal" can be very long-lived, for instance, because of pinning by surface irregularities. The slab geometry could also help to halt coarsening when the size of the domains exceeds the slab thickness. The critical velocity of vortex nucleation in the presence of a domain wall is smaller than in a uniform texture; therefore we would expect vortices to get nucleated in walls and get transported along their network. As the vortices have to pass through multiple three-way junctions possessing potential barriers, the vortex mobility (and hence final distribution of vorticity) should be affected by them. In the illustration in Fig. 1, the vortices will experience a barrier impeding their transport along the l wall and ld wall (from left to right or vice versa), they will also get trapped in the "pocket" in the center if they are forced to move downwards (because d walls can not carry vorticity). After the rotation is stopped, the vortices will tend to leave the cell; however, some will remain trapped at the amount limited either by the height of those potential barriers or the creation of antivortices which would annihilate the trapped ones. The experiment points at the latter process as the relevant one. For $\Omega_0 = 0.026$ rad/s (i.e., total $N_{\text{trap}} = 62$), the average distance between vortices is about 1 mm, which makes it plausible that there are enough domain walls to accommodate them all. It would be of interest to see if Ω_0 will be much smaller in a wider slab, $D \gg 1$ mm, where there might not be enough domain walls to pin that many vortices.

To conclude, strong intrinsic pinning of vorticity by multidomain textures is observed in ^{3}He-A in a slab. The amount of trapped vorticity is universal for different densities of domain walls and slab thicknesses. Thanks to this pinning, the existence of substantial persistent current was demonstrated in a simply connected slab. A model of the critical state set by the critical velocity for vortex nucleation explains the observed hysteretic loops.

We acknowledge discussions with H. E. Hall and the contributions of S. May and D. J. Cousins in the construction and improvement of the apparatus. Support was provided by EPSRC under GR/N35113 and GR/R94855.

[1] G. Blatter *et al.*, Rev. Mod. Phys. **66**, 1125 (1994).
[2] P. Hakonen *et al.*, Phys. Rev. Lett. **81**, 3451 (1998).
[3] J. H. Durrell *et al.*, Phys. Rev. Lett. **90**, 247006 (2003).
[4] M. Tomita and M. Murakami, Nature (London) **421**, 517 (2003).
[5] M. Sigrist and D. F. Agterberg, Prog. Theor. Phys. **102**, 965 (1999).
[6] E. Dumont and A. C. Mota, Phys. Rev. B **65**, 144519 (2002).
[7] D. Vollhardt and P. Wölfle, *The Superfluid Phases of Helium 3* (Taylor & Francis, London, 1990).
[8] O. V. Lounasmaa and E. Thuneberg, Proc. Nat. Acad. Sci. U.S.A. **96**, 7760 (1999).
[9] P. M. Walmsley *et al.*, Phys. Rev. Lett. **91**, 225301 (2003).
[10] P. J. Hakonen *et al.*, Phys. Rev. Lett. **58**, 678 (1987).
[11] P. L. Gammel *et al.*, Phys. Rev. Lett. **55**, 2708 (1985).
[12] This differs for thin slabs considered in M. M. Salomaa and G. E. Volovik, J. Low Temp. Phys. **74**, 319 (1989).
[13] T. D. C. Bevan *et al.*, J. Low Temp. Phys. **109**, 423 (1997).
[14] J. Kopu *et al.*, Phys. Rev. B **62**, 12 374 (2000).
[15] U. Parts *et al.*, Phys. Rev. Lett. **72**, 3839 (1994).